Investigating the optical degradation of InAs quantum dot lasers on silicon through combined electro-optical characterization and gain measurements

PAPER • OPEN ACCESS

Investigating the optical degradation of InAs quantum dot lasers on silicon through combined electro-optical characterization and gain measurements

To cite this article: Michele Zenari *et al* 2025 *J. Phys. Photonics* **7** 025007

Journal of Physics: Photonics

OPEN ACCESS

RECEIVED
8 November 2024

REVISED
2 February 2025

ACCEPTED FOR PUBLICATION
11 February 2025

PUBLISHED
20 February 2025

PAPER

Investigating the optical degradation of InAs quantum dot lasers on silicon through combined electro-optical characterization and gain measurements

Michele Zenari[1,*], Marco Novarese[6], Matteo Buffolo[1], Carlo De Santi[1], Justin Norman[4], Eamonn T Hughes[4], John E Bowers[3,4], Robert W Herrick[5], Mariangela Gioannini[6], Gaudenzio Meneghesso[1], Enrico Zanoni[1] and Matteo Meneghini[1,2]

[1] Department of Information Engineering, University of Padova, 35131 Padova, Italy
[2] Department of Physics and Astronomy, University of Padova, via Marzolo 8, 35131 Padova, Italy
[3] Department of Electrical and Computer Engineering, University of California, Santa Barbara, CA 93106, United States of America
[4] Materials Department, University of California, Santa Barbara, CA 93106, United States of America
[5] Robert Herrick Consulting, San Jose, CA 95117, United States of America
[6] Department of Electronics and Telecommunication, Politecnico di Torino, 10129 Torino, Italy
[*] Author to whom any correspondence should be addressed.

E-mail: michele.zenari@unipd.it

Keywords: degradation, quantum-dot laser, gain spectra, modeling

Abstract

We evaluate the degradation of 1.3 μm InAs quantum-dot laser diodes epitaxially grown on silicon. For the first time, the optical degradation mechanisms are investigated by evaluating the variations in the gain spectra measured during a constant-current stress test. Remarkably, the gain spectra showed that the reduction in the peak modal gain is dominant compared to the increase in internal absorption losses. Moreover, the increase in threshold current (I_{th}) induced by stress was found to be correlated to the gain peak reduction. This experimental evidence was investigated by modeling the peak modal gain variation through a rate equation model. The outcome of this activity confirms that the variation of both I_{th} and modal gain can be explained solely by the reduction in injection efficiency, caused by the stress-induced increase in non-radiative recombination centers (NRRCs). This result supports previous findings on the optical degradation of 1.3 μm InAs quantum dot lasers, which is ultimately ascribed to the increase in concentration of NRRCs within the active region.

1. Introduction

The telecommunications field is facing novel challenges arising from the expansion of 5G infrastructures, growing demands for data traffic, and the evolution of high-speed, cost-effective, data transmission systems [1–4]. Silicon photonics (SiPh) has the potential to boost a variety of integrated systems, not only in datacom and telecom applications [5] but also in biphotonic systems [6], LiDARs [7], and ultimately in photon-based quantum computing systems [8]. The commercialization of SiPh devices is based on highly efficient and reliable electrically-pumped laser diodes [9]. Due to the lack of efficient Si-based IR emitters, these laser diodes are typically based on III–V materials: a crucial factor is therefore the compatibility of these semiconductors with Si-based substrates. There are several integration techniques, such as heterogeneous integration [10] and micro transfer printing [11], and one promising approach involves the direct growth of III–V materials onto Si substrates [12, 13]. Nevertheless, significant challenges arise from the large lattice constant mismatch, the different thermal expansion coefficients, and the antiphase domains, resulting in the formation of dislocations and, ultimately, non-radiative recombination centers (NRRCs) [14, 15]. Indeed, during operation such defects can grow and propagate via recombination enhanced defect reaction mechanisms [16, 17]. This ultimately leads to sub-optimal laser performance and to a limited lifespan [18]. A novel solution to mitigate this issue is to employ quantum dots (QDs) as the optical gain medium in the

active region. Owing to their unique properties, QDs are less vulnerable to crystalline defects, resulting in enhanced reliability [19].

To investigate the degradation of QD laser diodes (QD LDs), basic approaches are focused on the evaluation of both the optical (*L–I*, spectra) and electrical (*I–V, C–V*) characteristics. While these measurements are crucial for understanding the processes that lead to the worsening of the main output properties of the devices, they fail in providing information about relevant internal and operating parameters, such as the gain spectrum and internal absorption losses [20].

To fill this gap, in this work we evaluated for the first time the correlation between the electro-optical degradation of QD laser diodes, and the variations of the gain spectra. Although the literature includes other works that measure gain spectra during accelerated aging tests [21, 22], these studies focus solely on evaluating internal absorption losses without addressing variations across the entire gain spectrum. Our methodology enables us, for the first time, to discriminate between changes in internal absorption losses and degradation lowering of the gain peak. The analysis was carried out on devices epitaxially grown on silicon, which were subjected to an accelerated aging test. The analysis of the experimental results revealed a minor variation of internal absorption losses throughout the experiment. Conversely, the gain peak exhibited a decrease, which was found to be correlated with the increase in threshold current. By exploiting a simplified rate equation model, these experimental observations were ultimately attributed to the reduction in injection efficiency of the carriers in the QDs, in agreement with previous qualitative interpretations [23].

2. Devices under investigation

The devices analyzed in this work are InAs quantum-dot laser diodes epitaxially grown by molecular beam epitaxy (MBE) on silicon substrates. The samples are designed for emission at 1.3 μm. The epitaxial structure, reported in figure 1, is formed by a periodic active region enclosed within two GaAs wave-guiding layers and two $Al_{0.4}Ga_{0.6}As$ cladding layers, grown on top of a $\sim$3 μm thick GaAs buffer layer. The active region of the lasers is composed by seven equal dots-in-well (DWELL) layers, each featuring undoped GaAs barriers and a 10 nm thick Be-doped layer ($N_A = 5 \times 10^{17}$ cm^{-3}), separated from the $In_{0.15}Ga_{0.85}As$ well containing the layer of self-assembled InAs QDs, whose areal density is around 5×10^{10} cm^{-2} (further details on the growth processes can be found in [24]). The processing of the devices was then completed with the etching of the 3.5 μm wide ridge down to the n-contact layer (figure 1), the thinning of the silicon substrate, and the cleaving of the facets (that were left as-cleaved after fabrication), to form a 850 μm long Fabry–Pérot optical cavity.

3. Methodology

For our experimental purposes, one representative device with threading dislocation density (TDD) of $7{\cdot}10^7$ cm^{-2} has been stressed and characterized on-wafer. Temperature control was achieved by means of a TEC-controlled baseplate. The electrical bias was provided by a source-meter. The optical measurements were carried out through a single-mode lensed optical fiber which was placed onto a hexapod to achieve optimized alignment with one of the output laser facets. The fiber was connected to a 1×2 optical splitter to redirect half of the optical emission to a Keysight 8136 A optical power meter, and half to a Yokogawa AQ6380 optical spectrum analyzer which has a maximum wavelength resolution of 5 pm. This configuration allows to perform fast and highly-repeatable *L–I* characterizations, while also being capable of acquiring high-resolution optical spectra below and above threshold with sufficient signal-to-noise (SNR) ratio (figure 2). The stress experiment was paused at different stages to evaluate the effects of device degradation by measuring both the *L–I* characteristics and optical spectra. Both stress and characterization were carried out at a fixed baseplate temperature of $T_{AMB} = 35$ °C. A constant current stress at 148 mA (5 kA cm^{-2}) was chosen to collect degradation data comparable with previous results obtained on similar devices [23, 25] (TDD = $7{\cdot}10^6$ cm^{-2}, three QD layers), and to induce a sufficient amount of degradation in a time frame of 180 h (i.e. about one week) [24]. The stress conditions differ from the actual operating conditions intended for the devices under test, where lasers are generally designed to provide a constant output power (COP). This kind of operating condition would imply a time-dependent increase in current during aging, to maintain a COP even in presence of degradation [26]. However, since degradation rate may depend on injected current and/or on the recombination rates [23], COP stress would result in a positive feedback and acceleration of the degradation process during operation, and this would prevent an accurate extraction of the acceleration factors. Additionally, the employed stress current (density), corresponding to about 150 mA ($\approx 4 \times I_{th}$), is higher compared to typical operating conditions ($2 \times$ to $3 \times I_{th}$), and our previous studies demonstrated that the degradation process and related acceleration factor do not change significantly if the sample operates below the threshold of excited-state emission [23].

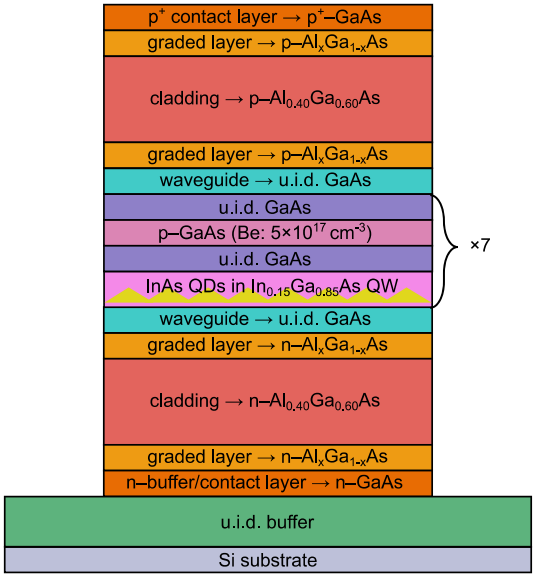

Figure 1. Epitaxial structure of the devices under investigation.

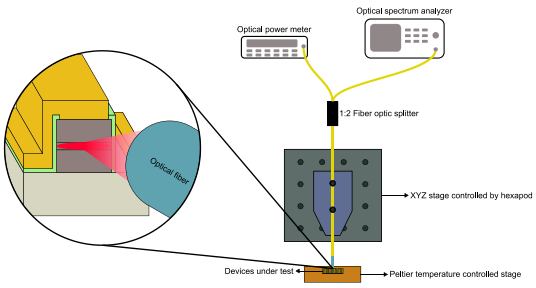

Figure 2. Schematic representation of the experimental setup.

4. Experimental results

4.1. Optical power vs current characteristics

The *L–I* characteristics acquired at different times of the aging procedure are depicted in figure 3. The plotted curves show an increase in the threshold current (I_{th}), highlighting a lowering in the optical power below threshold (OP_{sub}) and in the slope efficiency (SE), which are comparable with previous works [23]. Such degradation could be macroscopically interpreted as a reduction of the injection efficiency of carriers in the active region and/or increase of the internal absorption losses. The degradation kinetics, illustrated in figure 3(a), have been qualitatively discussed in our previous study on similar devices [14], and ascribed to the diffusion of NRRC close to the QDs. The increase in NRRCs promotes non-radiative Schokley–Reed Hall (SRH) recombination in the QW 2D reservoir [27], ultimately reducing the injection of carriers into the QDs. It was experimentally demonstrated that threading dislocations and misfit dislocations arising from material mismatch in the devices can evolve during aging [15, 28, 29]. The growth of these dislocations can increase the density of NRRCs near the active layers. The capture of carriers in the InGaAs wells, followed by SRH recombination, reduces the rate of carriers injected into the QDs relative to the total carriers injected into the device. We previously modeled this physical phenomenon [30] demonstrating the degradation of optical characteristics, such as the increase in threshold current and the reduction in SE and optical power below threshold.

4.2. Gain spectra measurements

To quantitatively support our degradation hypothesis, we employed the Hakki–Paoli method, which allowed us to extrapolate the net gain spectrum of the laser, as well its stress-induced variations. Throughout the characterization stages, we collected sub-threshold spectra at 20, 25, 30, and 35 mA (the I_{th} of the unaged device was ≈40 mA) to monitor their variation during stress: figure 4(a) reports a representative spectrum

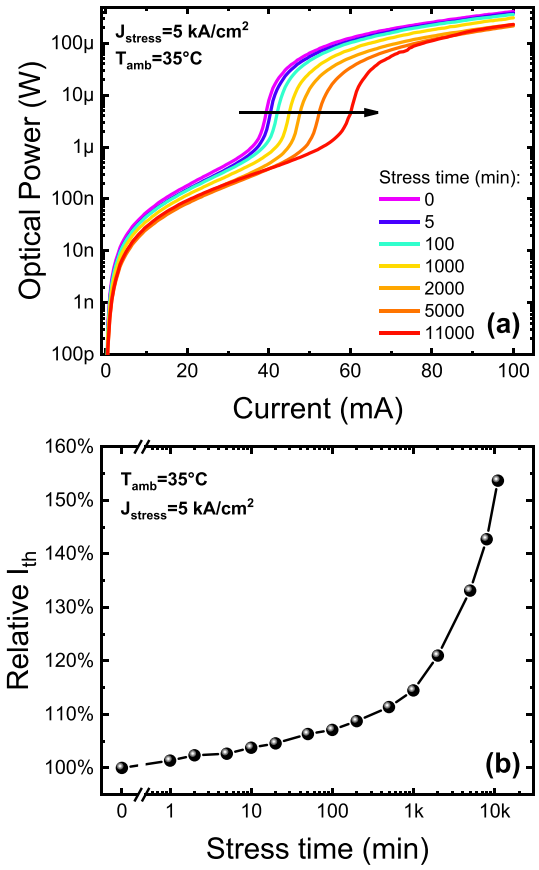

Figure 3. (a) Experimental L–I curves collected after each step of the stress experiment from which the threshold current was extrapolated. (b) Threshold current kinetics collected during the constant current stress experiment ($J_{stress} = 5$ kA cm^{-2}, $T_{amb} = 35$ °C).

acquired at 35 mA. To compute the gain spectrum of the laser at any current below the threshold current, we adopted the Hakki–Paoli method described in [20]. This method involves the evaluation of peaks and valleys in the laser spectrum, which can be seen in the zoomed-in view of figure 4(b). To determine the net gain, we started by calculating the mirror losses as:

$$\alpha_{\mathrm{m}} = \frac{1}{2L}\ln\left(\frac{1}{R_1 R_2}\right) \tag{1}$$

where R_1 and R_2 (facet reflectivities) are supposed to be equal and were calculated by taking into account the refractive index of air (n_{air}) and GaAs (n_{wg}) as:

$$R = \left(\frac{n_{\mathrm{wg}} - n_{\mathrm{air}}}{n_{\mathrm{wg}} + n_{\mathrm{air}}}\right)^2 \cong 0.32. \tag{2}$$

As a result, we calculated the net gain according to the following formula [20]:

$$g_{\mathrm{net}}(\lambda) = \frac{1}{L}\ln\left(\frac{\sqrt{\gamma_{\mathrm{i}}} - 1}{\sqrt{\gamma_{\mathrm{i}}} + 1}\right) - \frac{1}{2L}\ln\left(\frac{1}{R_1 R_2}\right) \tag{3}$$

where L is the cavity length, and γ_{i} represents the modulation depth, which can be written as [31]:

$$\gamma_{\mathrm{i}} = \frac{P_{\mathrm{i}}}{V_{\mathrm{i}}} \tag{4}$$

where γ_{i} represents the ratio between the intensity of a peak in the spectrum (P_{i}) and the intensity of the adjacent valley (V_{i}). The gain spectra, extrapolated with the Hakki–Paoli method during the stress experiment, are reported in figure 4(c); these are obtained by stressing the laser at the current of 5 kA cm^{-2} and measuring the spectra at different aging times at the current of 35 mA that is always below threshold.

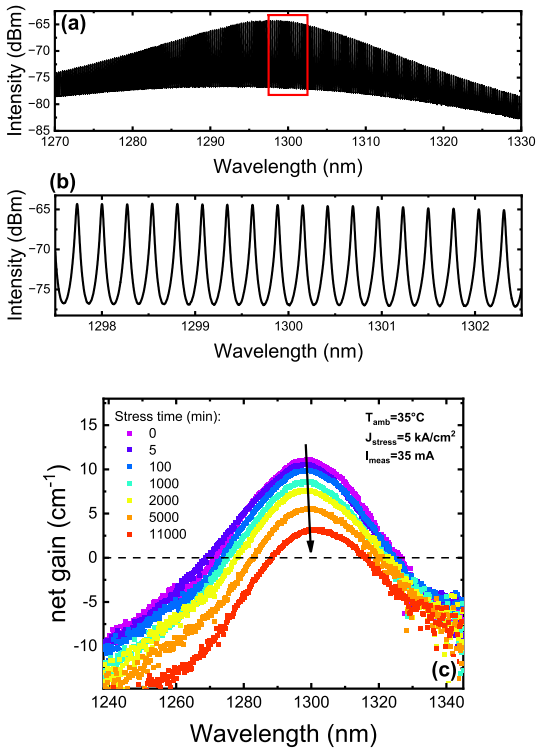

Figure 4. (a) Optical spectrum acquired at 35 mA in the case of the unaged device; (b) zoomed view of the central part of spectrum. The figure shows the good level of discrimination between peaks and valleys, which is required for the applicability of the Hakki–Paoli method. (c) Net gain extrapolated from the spectra acquired at different stages of the constant current stress test. The curves in the plot show both a reduction in peak gain and a decrease in the plateau around 1340 nm (related to the internal absorption losses). The resulting values of gain and internal absorption losses are in agreement with previous studies on similar devices [35].

The experimental curves show a strong variation in the net gain peak (around 1300 nm) during device aging, which decreases from 11 cm^{-1} to 2.5 cm^{-1}.

Another crucial factor in the study of gain spectra is the evaluation of the internal absorption losses (α_{int}). The optical losses have various contributions, the most important being scattering due to waveguide nonuniformities and free carrier (intraband) absorption [32]. The optical losses are typically measured from the plateau of the gain spectrum at longer wavelengths (i.e. at energies well below the bandgap). We calculate the internal absorption losses α_i by considering the following equation:

$$g_{net}(\lambda) = \Gamma G(\lambda) - \alpha_{int} \tag{5}$$

where Γ represents the optical confinement factor, $g_{net}(\lambda)$ is the net modal gain, and $G(\lambda)$ is the material gain. In equation (5), $g_{net}(\lambda)$ is computed experimentally through equation (3).

A simple approach to estimate the internal absorption losses can be followed by considering that the material gain asymptotically goes to zero at wavelengths much longer compared to the peak emission. Although $G(\lambda)$ is not exactly zero at long wavelengths, it can be small enough for an accurate measurement of α_{int} [33, 34].

The estimated internal absorption losses (extrapolated from the plateau around 1340 in figure 4(c)) exhibit a minor variation during the experiment, ranging from $\alpha_{int} \approx 5.5$ cm^{-1} (unaged) to $\alpha_{int} \approx 6.8$ cm^{-1} (post-stress). The increase in α_{int} is compatible with other works on similar devices [21, 22].

In order to better understand the degradation process, we reported the trend of the net gain peak as a function of the measuring current in figure 5(a). As expected, the dependence of net gain on current exhibits a consistent lowering, in agreement with the worsening of the optical characteristics occurring during the aging of the device. In particular, the net gain appears to decrease uniformly across all the tested measuring currents. By subtracting each curve from the first (unaged, 0 min) measurement, it is possible to observe a rigid shift of the curves, indicating that the characteristics does not feature a change in shape (see figure 5(b)). This ultimately indicates that the degradation mechanism responsible for the optical degradation affects the net gain peak more or less equivalently across the entire range of adopted testing currents.

In order to confirm the correlation between the degradation of the optical characteristics and the gain spectra, we plotted the relative net gain peak (at 35 mA) versus the relative I_{th} during the aging experiment.

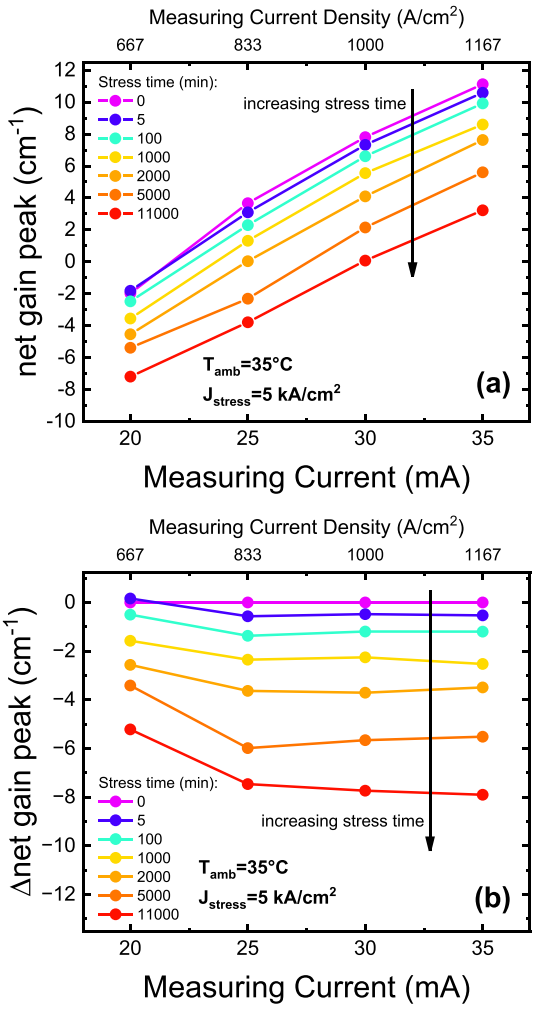

Figure 5. (a) Magnitude of the net gain peak vs current for different stress times. The curves show that the stress is responsible for the decrease in the net gain of the laser in different bias conditions. (b) The net gain vs current curves were subtracted from the 0 min curve to highlight the rigid shift in the characteristics during the stress experiments. At low bias (20 mA), detecting the signal was more challenging due to low signal-to-noise ratio (SNR). Therefore, the higher uncertainty results in some points not following a constant trend.

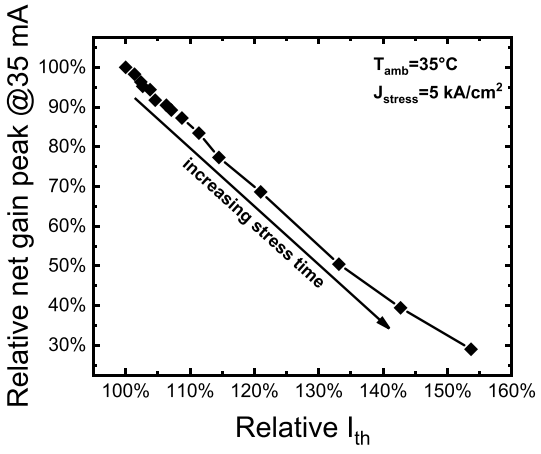

Figure 6. Correlation between the threshold current and the peak magnitude of the net gain.

The resulting graph, reported in figure 6, clearly shows a linear correlation among the two quantities, suggesting that the physical origin of the process responsible for the worsening of the *L–I* characteristics, and for the reduction in the net modal gain, is the same.

Table 1. List of parameters employed to model the optical characteristics of the laser above threshold. Note that v_g is the group velocity and n_g is the group refractive index. In addition, Γ refers to the confinement factor per each DWELL.

Symbol	Description	Value	Unit	References
q	Electron charge	$1.6{\cdot}10^{-19}$	(C)	
V	Active volume	$4.67{\cdot}10^{-11}$	(cm^3)	
$A=\frac{1}{\tau_{SRH}}$	SRH coeff.	$1/1{\cdot}10^{-9}$[a]	(s^{-1})	[37]
B	Radiative coeff.	$1.1{\cdot}10^{-10}$	($cm^3\ s^{-1}$)	[38]
C	Auger-Meitner coeff.	$1{\cdot}10^{-27}$	($cm^6\ s^{-1}$)	[39, 40]
a	Differential gain	$1.6{\cdot}10^{-16}$	(cm^2)	[41]
$g_0 = a{\cdot}v_g$	Gain slope constant	$1.34{\cdot}10^{-6}$	($cm^{-3}\ s^{-1}$)	
N_{tr}	Transparency carrier density	$1.15{\cdot}10^{18}$	(cm^{-3})	[42]
EPS	Gain compression factor	$1.5{\cdot}10^{-17}$	(cm^3)	[41]
Γ	Confinement Factor	0.02		[27]
$\tau_p = \frac{1}{(\alpha_m+\alpha_i)\frac{v_g}{n_g}}$	Photon lifetime	$8.56{\cdot}10^{-12}$	(s)	[35]
β	Spontaneous emission factor	$1{\cdot}10^{-4}$		[27]
η_{inj}	Injection efficiency	0.85		[35]

[a] The τ_{SRH} used in the simulation is consistent with the value shown in [35].

5. Modeling of the optical degradation

According to previous studies [18, 23–25, 35], the optical degradation of InAs QD LDs epitaxially grown on Si, featuring the DWELL structure is driven by the reduction in injection efficiency (η_{inj}). This process occurs through the recombination-enhanced generation/diffusion of defects inside the device active region. These defects act as NRRCs, effectively stealing carriers before they can be captured by QDs. To explain this process, we use a modified rate equation model to analyze the variation in the gain spectra exhibited during the stress test. The proposed model is valid for a QW laser, but the phenomenological considerations can also be applied to QD LDs [36]. The set of adopted carrier and photon rate equation is the following:

$$\begin{cases} \frac{dN}{dt} = \frac{\eta_{inj} I}{qV} - N\left(A + BN + CN^2\right) - g_0\left(N - N_{tr}\right)\frac{S}{1+EPS{\cdot}S} \\ \frac{dS}{dt} = \Gamma g_0\left(N - N_{tr}\right)\frac{S}{1+EPS{\cdot}S} - \frac{S}{t_p} + \Gamma\beta BN^2 \end{cases} \tag{6}$$

where S is the photon density, and all remaining parameters are described in table 1 involving results from other works on QD LDs as similar as possible to the DUTs analyzed within this work.

Since QDs are sandwiched between the wetting layer and the InGaAs well, to determine the active volume V we assumed an equivalent active volume of InAs QDs with a thickness of 2 nm. Actually, the real QD volume should be lower, as QDs do not form a continuous layer, but rather a dot-like textured surface [24].

Based on the parameters listed in table 1, we solved the equations reported in equation (6) to match the unaged net peak gain vs current curve (see figure 7), having the injection efficiency as the sole free parameter. As it is possible to see in the figure, by only modifying η_{inj} from 0.85 (initial estimated value, see [42]) to 0.6 (i.e. supposing a relative reduction of 15%), we were able to reproduce the post-stress net peak gain vs current curve. This confirms that the variation of η_{inj} alone can account for the experimentally observed reduction in the net modal gain in the laser. From a physical point of view, this demonstrates the importance of SRH recombination outside the QDs (in the InGaAs QWs), which subtracts carriers from the active region, lowering the equivalent injection efficiency of the QDs. A variation in the internal SRH recombination in the QDs (modeled by the parameter A in the differential equation) is also expected, but solely varying this parameter has been shown not to accurately emulate the optical degradation of the devices under investigation (for further details, refer to figure 6 in [30]).

In order to replicate the experimental correlation between the threshold current increment and the gain peak lowering (figure 6), we calculated the *L–I* curves and gain peak at 35 mA from the rate equation model. Figure 8 shows again that the variation in the injection efficiency alone (from 0.85 to 0.60) matches quite well with the experimental trend of I_{th} and gain. We can observe a small deviation between the experimental and simulated curves, especially for longer stress times. We cannot exclude the possibility that other parameters may also change during the aging process. For instance, the SRH rate in the QDs (A coefficient) or the internal absorption losses α_{int} may also vary (even though we measured only a slight variation in the latter parameter). Nonetheless, the aim of the modeling was to demonstrate that just the variation in injection efficiency itself can effectively explain most of the optical degradation exhibited by the devices.

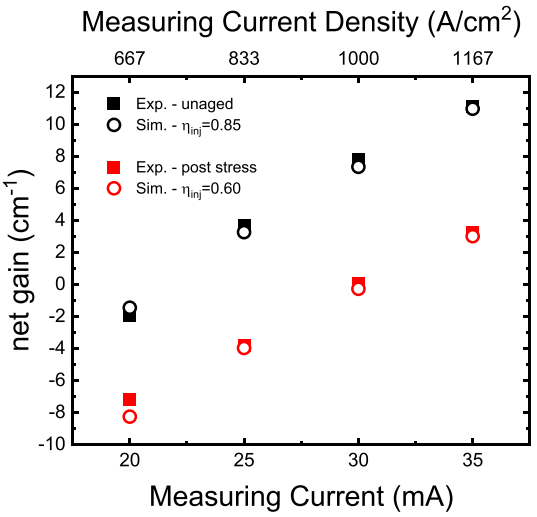

Figure 7. Net modal gain comparison: unaged vs post stress characteristics. The superposition of the experimental and simulated curves demonstrates the validity of the model and of the hypotheses adopted for the simulations.

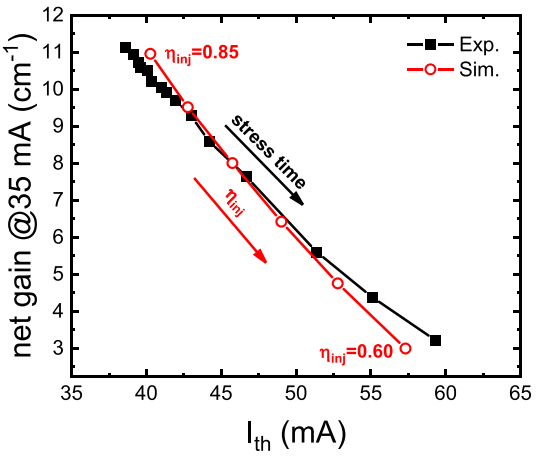

Figure 8. Comparison of the experimental and simulated relation between threshold current and net gain during aging. The simulated curve, in red, shows that the experimental behavior can be described by only adjusting the injection efficiency.

6. Conclusions

We analyzed the degradation of 1.3 μm QD lasers grown on silicon. For the first time, we employed the measurement of the gain spectra during an aging experiment to assess the physical origin of device degradation. The variations exhibited by the gain spectra during a constant-current stress showed that (i) the decrease in magnitude of the gain peak represents the major spectral feature variation during aging, (ii) the internal absorption losses exhibit a moderate variation (from 5.5 to 6.8 cm^{-1}), and (iii) that the threshold current increase is correlated with the lowering in the modal gain peak during the stress experiment.

By comparing this experimental evidence to a rate-equation model, we conclude that the worsening in both threshold current and gain can be ascribed to the lowering of injection efficiency, in agreement with previous reports on similar samples. The methodology proposed in this work ultimately introduces a novel approach to identify the origin of the optical degradation of a generic laser diode based on the evaluation of its stress-time dependent gain spectra.

Data availability statement

All data that support the findings of this study are included within the article (and any supplementary files).

ORCID iDs

Michele Zenari https://orcid.org/0000-0001-8803-3824
Matteo Buffolo https://orcid.org/0000-0002-9255-6457
Robert W Herrick https://orcid.org/0009-0008-2230-6357

References

[1] Helkey R, Saleh A A M, Buckwalter J and Bowers J E 2019 High-performance photonic integrated circuits on silicon *IEEE J. Sel. Top. Quantum Electron.* **25** 1–15
[2] Sabella R 2020 Silicon photonics for 5G and future networks *IEEE J. Sel. Top. Quantum Electron.* **26** 1–11
[3] Wan Y *et al* 2021 High speed evanescent quantum-dot lasers on Si *Laser Photon. Rev.* **15** 2100057
[4] Liu S, Wu X, Jung D, Norman J C, Kennedy M J, Tsang H K, Gossard A C and Bowers J E 2019 High-channel-count 20 GHz passively mode-locked quantum dot laser directly grown on Si with 41 Tbit/s transmission capacity *Optica* **6** 128
[5] Zhang C and Bowers J E 2018 Silicon photonic terabit/s network-on-chip for datacenter interconnection *Opt. Fiber Technol.* **44** 2–12
[6] Dhote C, Singh A and Kumar S 2022 Silicon photonics sensors for biophotonic applications—a review *IEEE Sens. J.* **22** 18228–39
[7] Hashemi H 2022 A review of silicon photonics LiDAR *Proc. Custom Integrated Circuits Conf.* (*April 2022*)
[8] Mikulics M and Hardtdegen H H 2020 Fully photon operated transmistor/all-optical switch based on a layered $Ge_1Sb_2Te_4$ phase change medium *FlatChem* **23** 100186
[9] Buffolo M, De Santi C, Norman J, Shang C, Bowers J E, Meneghesso G, Zanoni E and Meneghini M 2021 A review of the reliability of integrated ir laser diodes for silicon photonics *Electron* **10** 2734
[10] Komljenovic T, Davenport M, Hulme J, Liu A Y, Santis C T, Spott A, Srinivasan S, Stanton E J, Zhang C and Bowers J E 2016 Heterogeneous silicon photonic integrated circuits *J. Light Technol.* **34** 20–35
[11] Roelkens G *et al* 2022 Micro-transfer printing for heterogeneous Si photonic integrated circuits *IEEE J. Sel. Top. Quantum Electron.* **29** 1–14
[12] Pan S, Cao V, Liao M, Lu Y, Liu Z, Tang M, Chen S, Seeds A and Liu H 2019 Recent progress in epitaxial growth of III–V quantum-dot lasers on silicon substrate *J. Semicond.* **40** 101302
[13] Tang M, Park J-S, Wang Z, Chen S, Jurczak P, Seeds A and Liu H 2019 Integration of III–V lasers on Si for Si photonics *Prog. Quantum Electron.* **66** 1–18
[14] Du A Y, Li M F, Chong T C, Xu S J, Zhang Z and Yu D P 1997 Investigation of dislocations and traps in MBE grown p-InGaAs/GaAs heterostructures *Thin Solid Films* **311** 7–14
[15] Selvidge J, Norman J, Salmon M E, Hughes E T, Bowers J E, Herrick R and Mukherjee K 2019 Non-radiative recombination at dislocations in InAs quantum dots grown on silicon *Appl. Phys. Lett.* **115** 131102
[16] Kimerling L C 1978 Recombination enhanced defect reactions *Solid-State Electron.* **21** 1391–401
[17] Liu A Y, Herrick R W, Ueda O, Petroff P M, Gossard A C and Bowers J E 2015 Reliability of InAs/GaAs quantum dot lasers epitaxially grown on silicon *IEEE J. Sel. Top. Quantum Electron.* **21** 690–7
[18] Buffolo M, Samparisi F, De Santi C, Jung D, Norman J, Bowers J E, Herrick R W, Meneghesso G, Zanoni E and Meneghini M 2019 Physical origin of the optical degradation of InAs quantum dot lasers *IEEE J. Quantum Electron.* **55** 1–7
[19] Norman J C, Jung D, Wan Y and Bowers J E 2018 Perspective: the future of quantum dot photonic integrated circuits *APL Photonics* **3** 30901
[20] Hakki B W and Paoli T L 1973 cw degradation at 300°K of GaAs double-heterostructure junction lasers. II. Electronic gain *J. Appl. Phys.* **44** 4113–9
[21] Liu J, Tang M, Deng H, Shutts S, Wang L, Smowton P M, Jin C, Chen S, Seeds A and Liu H 2022 Theoretical analysis and modelling of degradation for III–V lasers on Si *J. Appl. Phys.* **55** 9
[22] Shutts S, Allford C P, Spinnler C, Li Z, Sobiesierski A, Tang M, Liu H and Smowton P M 2019 Degradation of III–v quantum dot lasers grown directly on silicon substrates *IEEE J. Sel. Top. Quantum Electron.* **25** 1–6
[23] Buffolo M *et al* 2020 Investigation of current-driven degradation grown on silicon *IEEE J. Sel. Top. Quantum Electron.* **26** 1900208
[24] Jung D, Norman J, Kennedy M J, Shang C, Shin B, Wan Y, Gossard A C and Bowers J E 2017 High efficiency low threshold current 1.3 μm InAs quantum dot lasers on on-axis (001) GaP/Si *Appl. Phys. Lett.* **111** 122107
[25] Buffolo M, Lain F, Zenari M, De Santi C, Norman J, Bowers J E, Herrick R W, Meneghesso G, Zanoni E and Meneghini M 2022 Origin of the diffusion-related optical degradation of 1.3 μm InAs QD-LDs epitaxially grown on silicon substrate *IEEE J. Sel. Top. Quantum Electron.* **28** 1–9
[26] Shang C *et al* 2022 Electrically pumped quantum-dot lasers grown on 300 mm patterned Si photonic wafers *Light Sci. Appl.* **11** 1–8
[27] Saldutti M, Tibaldi A, Cappelluti F and Gioannini M 2020 Impact of carrier transport on the performance of QD lasers on silicon: a drift-diffusion approach *Photon. Res.* **8** 1388
[28] Hughes E T *et al* 2023 Dislocation-induced structural and luminescence degradation in InAs quantum dot emitters on silicon *Phys. Status Solidi a* **220** 2300114
[29] Hughes E T, Shang C, Selvidge J, Jung D, Wan Y, Herrick R W, Bowers J E and Mukherjee K 2024 Gradual degradation in InAs quantum dot lasers on Si and GaAs *Nanoscale* **16** 2966–73
[30] Zenari M, Buffolo M, De Santi C, Norman J, Hughes E T, Bowers J E, Herrick R, Meneghesso G, Zanoni E and Meneghini M 2023 Addressing the optical degradation of 1.3 μm quantum dot lasers through subthreshold characterization *ACS Photonics* **10** 4188–95
[31] Kunzmann D J, Wachs M, Uhlig L and Schwarz U T 2019 Comparison of different methods for optical gain spectroscopy *Jpn. J. Appl. Phys.* **58** SCCC05
[32] Henry C H, Logan R A, Merritt F R and Luongo J P 1983 The effect of intervalence band absorption on the thermal behavior of InGaAsP lasers *IEEE J. Quantum Electron.* **19** 947–52
[33] Avrutin E A, Chebunina I E, Eliachevitch I A, Gurevich S A, Portnoi M E and Shtengel G E 1993 TE and TM optical gains in AlGaAs/GaAs single-quantum-well lasers *Semicond. Sci. Technol.* **8** 80–87
[34] Ketelsen L J P 1994 Simple technique for measuring cavity loss in semiconductor lasers *Electron. Lett.* **30** 1422–4
[35] Jung D *et al* 2018 Highly reliable low-threshold inas quantum dot lasers on on-axis (001) Si with 87% injection efficiency *ACS Photonics* **5** 1094–100

[36] Cartledge J C and Srinivasan R C 1997 Extraction of DFB laser rate equation parameters for system simulation purposes *J. Light Technol.* **15** 852–60
[37] Liu Z *et al* 2020 Origin of defect tolerance in InAs/GaAs quantum dot lasers grown on silicon *J. Light Technol.* **38** 240–8
[38] GeFmont B L, Sokolova Z N and Yassievich I N 1982 *Sov. Phys. Semicond.* **16** 592–600
[39] Ghosh S, Bhattacharya P, Stoner E, Singh J, Jiang H, Nuttinck S and Laskar J 2001 Temperature-dependent measurement of Auger recombination in self-organized $In_{0.4}Ga_{0.6}As$/GaAs quantum dots *Appl. Phys. Lett.* **79** 722
[40] Novikov I I, Gordeev N Y, Maksimov M V, Shernyakov Y M, Semenova E S, Vasil'Ev A P, Zhukov A E, Ustinov V M and Zegrya G G 2005 Temperature dependence of the effective coefficient of Auger recombination in 1.3 μm InAs/GaAs QD lasers *Semiconductor* **39** 481–4
[41] Fiore A and Markus A 2007 Differential gain and gain compression in quantum-dot lasers *IEEE J. Quantum Electron.* **43** 287–94
[42] Wada K, Yoshioka H, Zhu J, Matsuyama T and Horinaka H 2011 Simple form of multimode laser diode rate equations incorporating the band filling effect *Opt. Express* **19** 3019